
1ST PLACE SOLUTION FOR ICDAR 2021 COMPETITION ON MATHEMATICAL FORMULA DETECTION

Yuxiang Zhong¹, Xianbiao Qi¹, Shanjun Li¹, Dengyi Gu¹, Yihao Chen¹, Peiyang Ning¹, and Rong Xiao¹

¹ Visual Computing Group (VCGroup), Ping An Property & Casualty Insurance Company.

July 13, 2021

ABSTRACT

In this technical report, we present our 1st place solution for the ICDAR 2021 competition on mathematical formula detection (MFD)². The MFD task has three key challenges, i.e. a large scale span, large variation of the ratio between height and width, and rich character set and mathematical expressions. Considering these challenges, we used Generalized Focal Loss (GFL), an anchor-free method, instead of the anchor-based method, and prove the Adaptive Training Sampling Strategy (ATSS) and proper Feature Pyramid Network (FPN) can well solve the important issue of scale variation. Meanwhile, we also found some tricks, e.g., Deformable Convolution Network (DCN), SyncBN, and Weighted Box Fusion (WBF), were effective in MFD task. **Our method was ranked 1st place in the final 15 teams.**

1 Introduction

Digitization of document images is vital for enabling searching in massive collections of digitized printed scientific documents. Different from common text content, general OCR software fails to process mathematical formulas. Usually, a specific mathematical expression recognition is needed for mathematical formulas. To do this, we have to detect the regions of mathematical formulas. The ICDAR 2021 competition on mathematical formula detection (MFD) is targeting this problem. In the MFD task, there are two forms of formulas, i.e. embedded and isolated.

Different from general object detection [1, 2, 3, 4, 5], the MFD task [6, 7, 8] has three key characteristics, i.e. large scale variance especially between isolated and embedded formulas, large variation of the ratio between width and height, and rich character set and mathematical expressions. In this paper, we fully consider the features of the MFD task, and develop an empirical solution that is ranked 1st place in the ICDAR 2021 competition on mathematical formula detection. In our solution, we used an anchor-free framework, Generalized Focal Loss (GFL) [9], instead of the anchor-based model [4] because the proposal generated by the latter is hard to cover different scales and different ratios between width and height. Meanwhile, we employed an adaptive training sample selection (ATSS) [10] to balance the sampled positive points on each formula instance. In addition, we leveraged the feature pyramid network (FPN) [11], the large input resolution, and the deformable convolutional network (DCN) [12] because these techniques could benefit large formula detection or small formula detection, or both. Finally, some other tricks, such as ResNeSt [13], SyncBN [14], the large batch size and the weighted box fusion (WBF) [15], Ranger [16] optimizer, were adopted in our solution.

*Xianbiao Qi is the corresponding author. If you have any questions or concerns about the implementation details, please do not hesitate to contact 1701210384@pku.edu.cn or qixianbiao@gmail.com.

²<http://transcriptorium.eu/~htrcontest/MathsICDAR2021/>

which after substitution in Eq. (12) leads to

$$\tau^2 - D\beta^2 = \frac{d_k^2 R_0^2}{4}. \quad (14)$$

In these coordinates the dilaton, or equivalently the string coupling squared, is $g_s^2 = e^{2\phi} = M^{-1} \eta^D R^{2d}$ and the Kalb-Ramond field strength is $H = \mathcal{N} R^d dt \wedge \mathcal{J}$.

Although there is a world of possibilities in the above class of solutions, perhaps the most interesting case is the one where $\mathcal{E}_s = 1$, since then the uncompactified part of spacetime is just Minkowski space: Taking $\mathcal{E}_s = 1$ for convenience, one finds that the solution in, string, cosmological time, reads

$$\begin{aligned} ds^2 &= d\tau^2 - d\vec{x}_{(D)}^2 - 2R_0^2 B(\tau)^{-1} d\tau_{\text{breath}} dy^m dy^n, \\ e^{2\phi} &= (\sqrt{2}R_0)^{d_k} \tau^{-1} B(\tau)^{-d_k/2}, \\ H &= \mathcal{N} R_0^{d_k/2} \tau^{-1} B(\tau)^{-2} d\tau \wedge \mathcal{J}, \\ B(\tau) &= \tau^{2/\sqrt{d_k}} + \tau^{-2/\sqrt{d_k}}. \end{aligned} \quad (15)$$

As one can see, this is a completely regular solution, modulo the usual gravitational singularities, which smoothly interpolates between two Kasner-like regions [6]. From the lower dimensional point of view, the Ansatz considered above corresponds to a solution of dilaton-gravity coupled to moduli [10], where the breathing mode, \mathcal{E}_s , and \mathcal{J} are the scalar fields parameterizing an $SU(2, \mathbb{R})/U(1)$ coset model. When $\mathcal{E}_s = 1$, the above solutions can be obtained from the solutions given in [2] by applying an $SU(2, \mathbb{R})$ transformation on the moduli.

2 RR case

In much the same way as in the foregoing subsection, we can use the RR two form in type IIA, to trigger compactification. In this case the equations of motion and the Bianchi identity imply that

$$F_{(2)} = \mathcal{N} \mathcal{J} = \frac{1}{2} \mathcal{N} \mathcal{J}_{mn} dy^m \wedge dy^n. \quad (17)$$

Applying the same steps as in the foregoing paragraph, one finds

$$\begin{aligned} 0 &= (d \log R)'' + \frac{(d_k - 4) \mathcal{N}^2}{8} M \eta^D R^{d_k - 4}, & (18) \\ 0 &= (d \log \eta)'' + \frac{d_k \mathcal{N}^2}{8} M \eta^D R^{d_k - 4} - \lambda \eta^{-2} M^2, & (19) \\ 0 &= (d \log M)'' - \frac{d_k \mathcal{N}^2}{8} M \eta^D R^{d_k - 4} - D \lambda \eta^{-2} M^2, & (20) \\ 0 &= [(d \log M)']^2 - D [(d \log \eta)']^2 - d_k [(d \log R)']^2 - \frac{d_k \mathcal{N}^2}{4} M \eta^D R^{d_k - 4} - D \lambda M^2 \eta^{-2}. & (21) \end{aligned}$$

Looking at the above expressions, one sees that they simplify enormously when one considers the case $\mathcal{E}_s = 1$: In that case the Kähler breathing mode decouples completely and one has $R = R_0 e^{2\phi}$. Equating also the powers of \mathcal{E}_s and \mathcal{J} in the equations, i.e. putting $M = \eta^{D/2}$, one necessarily has to impose

$$\lambda = \frac{\mathcal{N}^2}{4} (D + 3). \quad (22)$$

which after substitution in Eq. (12) leads to

$$\tau^2 - D\beta^2 = \frac{d_k \mathcal{N}^2 R_0^2}{4}. \quad (14)$$

In these coordinates the dilaton, or equivalently the string coupling squared, is $g_s^2 = e^{2\phi} = M^{-1} \eta^D R^{2d}$ and the Kalb-Ramond field strength is $H = \mathcal{N} R^d dt \wedge \mathcal{J}$.

Although there is a world of possibilities in the above class of solutions, perhaps the most interesting case is the one where $\mathcal{E}_s = 1$, since then the uncompactified part of spacetime is just Minkowski space: Taking $\mathcal{E}_s = 1$ for convenience, one finds that the solution in, string, cosmological time, reads

$$\begin{aligned} ds^2 &= d\tau^2 - d\vec{x}_{(D)}^2 - 2R_0^2 B(\tau)^{-1} h_{mn} dy^m dy^n, \\ e^{2\phi} &= (\sqrt{2}R_0)^{d_k} \tau^{-1} B(\tau)^{-d_k/2}, \\ H &= \mathcal{N} R_0^{d_k/2} \tau^{-1} B(\tau)^{-2} d\tau \wedge \mathcal{J}, \\ B(\tau) &= \tau^{2/\sqrt{d_k}} + \tau^{-2/\sqrt{d_k}}. \end{aligned} \quad (15)$$

As one can see, this is a completely regular solution, modulo the usual gravitational singularities, which smoothly interpolates between two Kasner-like regions [6]. From the lower dimensional point of view, the Ansatz considered above corresponds to a solution of dilaton-gravity coupled to moduli [10], where the breathing mode, \mathcal{E}_s , and \mathcal{J} are the scalar fields parameterizing an $SU(2, \mathbb{R})/U(1)$ coset model. When $\mathcal{E}_s = 1$, the above solutions can be obtained from the solutions given in [2] by applying an $SU(2, \mathbb{R})$ transformation on the moduli.

2 RR case

In much the same way as in the foregoing subsection, we can use the RR two form in type IIA, to trigger compactification. In this case the equations of motion and the Bianchi identity imply that

$$F_{(2)} = \mathcal{N} \mathcal{J} = \frac{1}{2} \mathcal{N} \mathcal{J}_{mn} dy^m \wedge dy^n. \quad (17)$$

Applying the same steps as in the foregoing paragraph, one finds

$$\begin{aligned} 0 &= (d \log R)'' + \frac{(d_k - 4) \mathcal{N}^2}{8} M \eta^D R^{d_k - 4}, & (18) \\ 0 &= (d \log \eta)'' + \frac{d_k \mathcal{N}^2}{8} M \eta^D R^{d_k - 4} - \lambda \eta^{-2} M^2, & (19) \\ 0 &= (d \log M)'' - \frac{d_k \mathcal{N}^2}{8} M \eta^D R^{d_k - 4} - D \lambda \eta^{-2} M^2, & (20) \\ 0 &= [(d \log M)']^2 - D [(d \log \eta)']^2 - d_k [(d \log R)']^2 - \frac{d_k \mathcal{N}^2}{4} M \eta^D R^{d_k - 4} - D \lambda M^2 \eta^{-2}. & (21) \end{aligned}$$

Looking at the above expressions, one sees that they simplify enormously when one considers the case $\mathcal{E}_s = 1$: In that case the Kähler breathing mode decouples completely and one has $R = R_0 e^{2\phi}$. Equating also the powers of \mathcal{E}_s and \mathcal{J} in the equations, i.e. putting $M = \eta^{D/2}$, one necessarily has to impose

$$\lambda = \frac{\mathcal{N}^2}{4} (D + 3). \quad (22)$$

Figure 1: Comparison of random sampling strategy and ATSS sampling. Left. positive samples with random sampling strategy; Right. positive samples with ATSS.

2 Challenge

Compared to general object detection in natural images or scene text detection in documents, mathematical formula detection in this task will encounter some specific difficulties. As shown in Figure 1, these challenges include

- a large scale span between embedded formula and isolated formula. The areas of some large isolated formulas are hundreds of times larger than that of some embedded formulas;
- huge variation of the ratio between height and width. As shown in Figure 1, the ratios range from around 0.5 to 12;
- rich character set and mathematical expressions. There are hundreds of mathematical characters, and their combinations are extremely rich.

The large scale span of formulas and the huge variation of the ratio between height and width will lead to a classical scale problem in object detection. To be specific, as shown in the left of Figure 1, isolated formulas with large area will obtain large number of positive samples, but small embedded formulas only have a few or even none of positive samples under the random sampling strategy. In addition, large scale span will bring in a challenge to the head of the detector. To deal with this issue, attention needs to be paid to the choice of the pyramid of the detector head. In the following section, we will describe methods targeting these two challenges.

3 Method

We treated this task as a pure object detection task, and adopted Generalized Focal Loss (GFL [9]) framework as our baseline. GFL is built on a Fully Convolutional One-Stage (FCOS) [17] detector that is a robust anchor-free method. Based on the up-mentioned challenges, we reckon the anchor-free method is better than the anchor-based methods (e.g.,

Faster R-CNN [4], Cascade R-CNN [5]) in this task. In the following, we will describe two key modules in detail that greatly improved our solution.

ATSS. Adaptive Training Sample Selection [10] is an effective sampling strategy to alleviate the complex artificial design of sampling ratio between positive and negative, and overcomes the sampling imbalance disadvantage of random strategy. As shown in the left of the Figure 1, the results of random sampling strategy obey an uniform distribution according to the area of positive samples. It means that larger formula will obtain more positive samples, while some tiny formulas will only get a few or even zero positive samples. The sampling frequency of these tiny embedded formulas is much lower than the large isolated formulas. Obviously, there is a sampling imbalance between tiny and large formulas with random sampling strategy. On the contrary, when using ATSS, the number of positive samples has no relationship with the area of instance. Each instance will get the same number of positive samples. As shown in the right of the Figure 1, ATSS can effectively eliminate the impact of imbalanced sampling.

FPN. Feature Pyramid Network (FPN) [11] is to explicitly address the problem of large scale span. The MFD task contains a large number of extremely small formulas, which bring great challenges to our model. As illustrated in Figure 2, for such a single extremely small character formula, their short sides are usually around 16 pixels. We observe that for any layer of FPN, the limit of the detector is 3 pixels. This means that if we use the default FPN (3-7), the short side of the formula needs to be at least 24 pixels to be detected. Obviously, there are many small embedded formulas that do not satisfy this condition. So we change the selection of FPN level to (2-6) so that our model can overcome this defect.

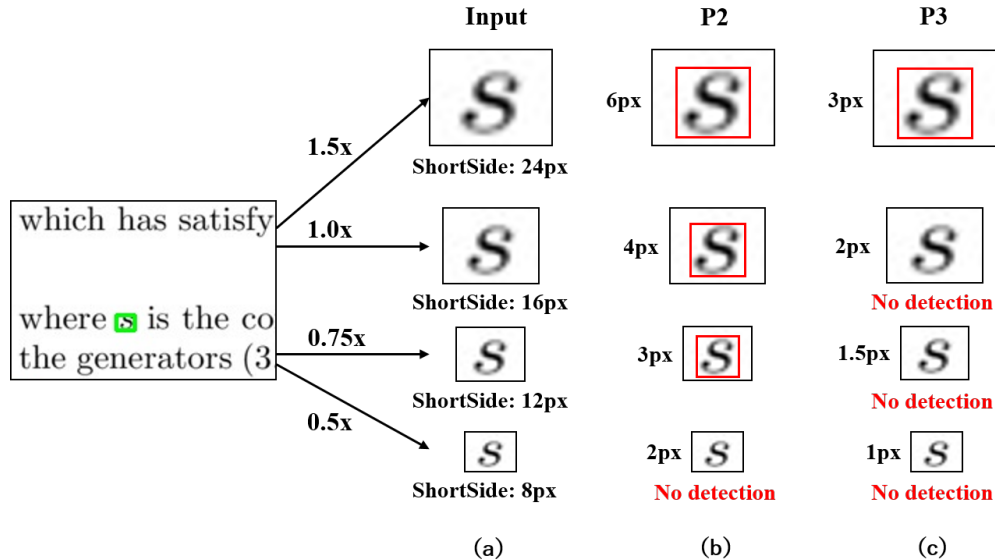


Figure 2: Illustration of the importance of the FPN on the MFD task. (a) Input size; (b) Corresponding size in P2; (c) Corresponding size in P3. Under some small scales, some positive samples will be missed.

4 Experiment

In this section, we will describe the implementation of our mathematical formula detection system in detail.

Dataset. Our used data is the official IBEM dataset. The IBEM dataset consists of 600 documents with a total number of 8,273 pages. There are 58,834 isolated and 260,323 embedded expressions. Each document contains approximately an average of 14 pages, 98 isolated mathematical expressions, and 434 embedded mathematical expressions. Each document is separated into individual pages with the corresponding ground truth. It is unknown how the organizers make a change to the original IBEM data set. Finally, there are 7,244 images with labels for training, and 4,028 images without a label for final evaluation. Only the provide training data is used for training.

Implementation Details. Our baseline model is GFL with ResNet101 [18] as the backbone. In the training of the baseline model, 8 Tesla V100 GPUs are used with batch size 2 in each GPU. The input image is resized equally to 1447×2048 with a keeping ratio. An 800×800 region is cropped from the original image. We use FPN (3-7) in default. In the baseline model, we use Adam [19] optimizer.

In the inference stage, we resize the test image to 1583×2048 due to the resolution distribution of the test dataset. Flip augment is turned on. For the post-processing, Non-Maximum Suppression (NMS) [20] with 0.6 IoU threshold is applied to filter the redundant box. All models are trained based on MMDetection [21] toolbox.

4.1 Ablation Study

We have conducted many attempts in this competition. Some effective tricks are listed below. We list these tricks according to the timeline we tried them.

Double Training Epoch. (DTE) Initially, We train 12 epochs. Then, we extend the training epoch to 24, and get a substantial score gain. Therefore, we further train 36 epochs, the result has no obvious change. It means that model is under-fitting with 12 epochs, and suitable with 24 epochs.

Large Crop Size. Considering that a small crop size will cause the long-isolated formula to be truncated sometimes. We decide to expand the crop size to 1440×1600 .

Random Flip is used at the training phase with a 0.5 ratios. In the inference phase, the image is also flipped as the input. The result is attained by mapping back the flipped boxes. The final result will be obtained by NMS.

ResNeSt [13] is used as our backbone to replace ResNet. Here, we use ResNeSt101 as the backbone.

Synchronized Batch Normalization (SyncBN) [14] is an effective batch normalization approach that is more suitable for the situation that the batch size is relatively small on each GPU graphics card.

Deformable Convolution Network (DCN) [12]. There are some discrete and large isolated formulas in the data set. To detect such formulas, a large receptive field is needed. Deformable convolution is an effective way to extend the receptive field. We replace all convolutions with deformable convolution layers from c3 to c5 in ResNeSt101.

Larger Batch Size (LBS). We expand batch size from 2 to 3 each GPU by utilizing the memory consume, such as mixed precision and replaced ReLU.

Ranger [16] is a synergistic optimizer combining RAdam (Rectified Adam) [22], LookAhead [23], and GC (gradient centralization) [24].

RegMax is a hyperparameter of GFL. It represents the largest position regression offset in each layer of FPN. In order to deal with the slim isolated formula, we increase the default 16 to 24.

FPN Selection. We change the FPN (3-7) to FPN (2-6).

Weight Box Fusion (WBF) [15] is used for model ensemble. It adopts an Expectation-Maximization algorithm to fuse the final bounding boxes. We select two models with the best performance which are trained initially with different random seeds. The IoU threshold of NMS is set to be 0.4 in WBF.

According to Table 1, we have the following observations.

- The number of training epochs should be large to make the model learn the data set fully.
- Large input resolution is good for the MFD task. Random crops from the images will cause the long-isolated formula to be truncated, and thus decrease the performance.
- ResNeSt is better than ResNet in this task. SyncBN can improve the performance a little.
- DCN is a powerful weapon in detection tasks. DCN largely improves the performance of the isolated formulas. Such improvement can be attributed to that DCN can extend the receptive field of the network. That is important for large isolated formulas.
- Ranger optimizer has outperformed Adam optimizer consistently. Similar observation is also found in our another report [25] about ICDAR 2021 Competition on Scientific Table Image Recognition to LaTeX [26]. In our evaluation of standard benchmarks, we also find that Ranger can improve the average accuracy by around 0.6%.
- The appropriate FPN level should be selected according to the scale of the object in the task. It can largely improve the performance.
- Weighted Box Fusion is useful in our task. It will improve the recall largely although it will slightly decrease the precision. Overall, it can improve the performance by 0.3%.

Remarks. Besides of the up-mentioned methods, we also tried many other approaches including CutMix data augmentation, soft NMS instead of the original NMS, IoU loss and GIoU loss instead of the smooth L1 loss, BFP and PAFPN instead of the original FPN, and Swish and Mish activation functions instead of ReLU. However, unfortunately, we did not observe obvious improvement on our validation set.

| DTE | LCS | Flip | NeSt | SyBN | DCN | LBS | Ranger | Reg 24 | FPN (2-6) | WBF | F1-score Embedded | F1-score Isolated | F1-score Total |
|-----|-----|------|------|------|-----|-----|--------|-----------|--------------|-----|--------------------------|--------------------------|---------------------------------|
| | | | | | | | | | | | 89.88 p:91.34 r:88.47 | 85.92 p:89.77 r:82.39 | 89.17 p:91.02 r:87.39 |
| ✓ | | | | | | | | | | | 91.36 p:92.80 r:89.96 | 86.29 p:90.93 r:82.10 | 90.45 p:92.26 r:88.71 |
| ✓ | ✓ | | | | | | | | | | 92.95 p:94.43 r:91.52 | 87.84 p:92.04 r:84.01 | 92.03 p:93.58 r:90.53 |
| ✓ | ✓ | ✓ | | | | | | | | | 93.58 p:94.79 r:92.41 | 88.38 p:92.29 r:84.78 | 92.66 p:94.35 r:91.03 |
| ✓ | ✓ | ✓ | ✓ | | | | | | | | 93.49 p:93.82 r:93.16 | 91.33 p:93.56 r:89.20 | 93.12 p:93.71 r:92.54 |
| ✓ | ✓ | ✓ | ✓ | ✓ | | | | | | | 93.81 p:94.00 r:93.63 | 91.60 p:93.82 r:89.48 | 93.42 p:93.97 r:92.89 |
| ✓ | ✓ | ✓ | ✓ | ✓ | ✓ | | | | | | 94.33 p:95.62 r:93.07 | 95.25 p:95.62 r:94.88 | 94.49 p:95.62 r:93.39 |
| ✓ | ✓ | ✓ | ✓ | ✓ | ✓ | ✓ | | | | | 94.58 p:95.16 r:94.00 | 95.60 p:95.97 r:95.23 | 94.76 p:95.31 r:94.22 |
| ✓ | ✓ | ✓ | ✓ | ✓ | ✓ | ✓ | ✓ | | | | 95.22 p:95.70 r:94.74 | 95.81 p:96.12 r:95.51 | 95.33 p:95.79 r:94.87 |
| ✓ | ✓ | ✓ | ✓ | ✓ | ✓ | ✓ | ✓ | ✓ | | | 95.01 p:95.86 r:94.16 | 97.28 p:97.18 r:97.38 | 95.41 p:96.10 r:94.73 |
| ✓ | ✓ | ✓ | ✓ | ✓ | ✓ | ✓ | ✓ | ✓ | ✓ | | 95.67 p:96.34 r:95.00 | 97.67 p:97.46 r:97.88 | 96.03 p:96.54 r:95.53 |
| ✓ | ✓ | ✓ | ✓ | ✓ | ✓ | ✓ | ✓ | ✓ | ✓ | ✓ | 96.01 p:95.79 r:96.23 | 98.14 p:97.32 r:98.98 | 96.33 p:96.81 r:95.85 |

Table 1: Experimental results of baseline, DTE (double training epoch), LCS (larger crop size), Flip (training and testing time flip), SyBN (SyncBN), DCN (deformable convolution network), LBS (larger batch size), Ranger optimizer, Reg 24 (a hyperparameter regmax), FPN (2-6) (FPN selection), WBF (weighted box fusion).

4.2 Final Results

The final results are shown on Table 2 reported by the organizers, and our team is PAPCIC (Visual Computing Group from Ping An Property & Casualty Insurance Company, China). The types, E, I, S characters, stand for Embedded, Isolated, and the Averaged, respectively. F1 score is used as the metric. Our method is ranked 1st place among all 15 teams. From Table 2, we found that

- almost all submissions obtained high performance on the isolated formula, but some methods performed poor on the embedded formula. The gap among the highest and the lowest on the isolated formula was around 3.0%, but this gap amounted to around 10.6% on the embedded formula. It means most algorithms can detect the isolated formulas well, and the main challenge of the MFD task lies on the detection of the embedded formula.
- compared to the “DLVCLab” and “TYAI” methods, our method slightly beat them on the isolated formula, but outperformed them largely on the embedded formula. We believe this improvement is attributed to the large input resolution, the ATSS and the proper FPN choice.

5 Conclusion

In this paper, we presented our 1st place method to ICDAR 2021 Competition on Mathematical Formula Detection. We built our approach on GFL, with ResNeSt as our backbone, to detect embedded and isolated formulas. We employed ATSS as our sampling strategy instead of random sampling to eliminate the effects of sample imbalance. Moreover, we observed and revealed the influence of different FPN levels on the detection result. Finally, with a series of useful tricks and model ensembles, our method was ranked 1st in the MFD task.

| Group ID | Type | F1 (Ts10+Ts11) | F1 Task dependent(Ts11) | F1 Task independent(Ts10) |
|----------|------|-------------------|----------------------------|------------------------------|
| PAPCIC | E | 94.89 | 95.11 | 94.64 |
| | I | 98.76 | 98.70 | 98.79 |
| | S | 95.47 | 95.68 | 95.37 |
| Lenovo | E | 94.29 | 93.98 | 94.44 |
| | I | 98.19 | 97.85 | 98.33 |
| | S | 94.96 | 94.60 | 95.13 |
| DLVCLab | E | 93.79 | 93.88 | 93.75 |
| | I | 98.54 | 98.61 | 98.51 |
| | S | 94.60 | 94.64 | 94.59 |
| TYAI | E | 93.39 | 93.94 | 93.13 |
| | I | 98.55 | 98.42 | 98.61 |
| | S | 94.28 | 94.66 | 94.10 |
| SPDBLab | E | 92.80 | 92.14 | 93.12 |
| | I | 98.06 | 97.76 | 98.19 |
| | S | 93.70 | 93.03 | 94.01 |
| YoudaoAI | E | 92.73 | 92.71 | 92.74 |
| | I | 98.34 | 98.38 | 98.32 |
| | S | 93.70 | 93.63 | 93.74 |
| PKUF-MFD | E | 91.94 | 92.32 | 91.76 |
| | I | 96.56 | 96.87 | 96.43 |
| | S | 92.72 | 93.04 | 92.57 |
| HW-L | E | 90.53 | 90.57 | 90.51 |
| | I | 98.94 | 98.61 | 99.08 |
| | S | 91.97 | 91.86 | 92.02 |
| Komachi | E | 90.39 | 89.69 | 90.72 |
| | I | 98.57 | 98.60 | 98.55 |
| | S | 91.79 | 91.11 | 92.10 |
| AIG | E | 89.71 | 89.19 | 89.95 |
| | I | 95.95 | 96.07 | 95.90 |
| | S | 90.75 | 90.26 | 90.97 |
| PKUSG | E | 89.10 | 88.59 | 89.34 |
| | I | 97.96 | 97.94 | 97.96 |
| | S | 90.62 | 90.09 | 90.87 |
| TAL | E | 87.87 | 88.51 | 87.57 |
| | I | 96.85 | 97.09 | 96.75 |
| | S | 89.42 | 89.89 | 89.19 |
| UIT | E | 86.04 | 85.64 | 86.23 |
| | I | 97.05 | 98.11 | 96.60 |
| | S | 87.94 | 87.63 | 88.08 |
| AV-DFKI | E | 85.35 | 84.75 | 85.63 |
| | I | 97.48 | 97.40 | 97.52 |
| | S | 87.45 | 86.80 | 87.76 |
| VH | E | 84.25 | 84.39 | 84.18 |
| | I | 98.59 | 98.51 | 98.62 |
| | S | 86.67 | 86.61 | 86.70 |

Table 2: Final results of all 15 teams on ICDAR 2021 Competition on Mathematical Formula Detection.

References

- [1] Ross Girshick. Fast r-cnn. In *Proceedings of the IEEE international conference on computer vision*, pages 1440–1448, 2015.
- [2] Joseph Redmon, Santosh Divvala, Ross Girshick, and Ali Farhadi. You only look once: Unified, real-time object detection. In *Proceedings of the IEEE conference on computer vision and pattern recognition*, pages 779–788, 2016.
- [3] Wei Liu, Dragomir Anguelov, Dumitru Erhan, Christian Szegedy, Scott Reed, Cheng-Yang Fu, and Alexander C Berg. Ssd: Single shot multibox detector. In *European conference on computer vision*, pages 21–37. Springer, 2016.
- [4] Shaoqing Ren, Kaiming He, Ross Girshick, and Jian Sun. Faster r-cnn: Towards real-time object detection with region proposal networks. *arXiv preprint arXiv:1506.01497*, 2015.
- [5] Zhaowei Cai and Nuno Vasconcelos. Cascade r-cnn: Delving into high quality object detection. In *Proceedings of the IEEE conference on computer vision and pattern recognition*, pages 6154–6162, 2018.
- [6] Mahshad Mahdavi, Richard Zanibbi, Harold Mouchere, Christian Viard-Gaudin, and Utpal Garain. Icdar 2019 crohme+ tfd: Competition on recognition of handwritten mathematical expressions and typeset formula detection. In *2019 International Conference on Document Analysis and Recognition (ICDAR)*, pages 1533–1538. IEEE, 2019.
- [7] Wei-Ta Chu and Fan Liu. Mathematical formula detection in heterogeneous document images. In *2013 conference on technologies and applications of artificial intelligence*, pages 140–145. IEEE, 2013.
- [8] Liangcai Gao, Xiaohan Yi, Yuan Liao, Zhuoren Jiang, Zuoyu Yan, and Zhi Tang. A deep learning-based formula detection method for pdf documents. In *2017 14th IAPR International Conference on Document Analysis and Recognition (ICDAR)*, volume 1, pages 553–558. IEEE, 2017.
- [9] Xiang Li, Wenhai Wang, Lijun Wu, Shuo Chen, Xiaolin Hu, Jun Li, Jinhui Tang, and Jian Yang. Generalized focal loss: Learning qualified and distributed bounding boxes for dense object detection. *arXiv preprint arXiv:2006.04388*, 2020.
- [10] Shifeng Zhang, Cheng Chi, Yongqiang Yao, Zhen Lei, and Stan Z Li. Bridging the gap between anchor-based and anchor-free detection via adaptive training sample selection. In *Proceedings of the IEEE/CVF Conference on Computer Vision and Pattern Recognition*, pages 9759–9768, 2020.
- [11] Tsung-Yi Lin, Piotr Dollár, Ross Girshick, Kaiming He, Bharath Hariharan, and Serge Belongie. Feature pyramid networks for object detection. In *Proceedings of the IEEE conference on computer vision and pattern recognition*, pages 2117–2125, 2017.
- [12] Jifeng Dai, Haozhi Qi, Yuwen Xiong, Yi Li, Guodong Zhang, Han Hu, and Yichen Wei. Deformable convolutional networks. In *Proceedings of the IEEE international conference on computer vision*, pages 764–773, 2017.
- [13] Hang Zhang, Chongruo Wu, Zhongyue Zhang, Yi Zhu, Haibin Lin, Zhi Zhang, Yue Sun, Tong He, Jonas Mueller, R Manmatha, et al. Resnest: Split-attention networks. *arXiv preprint arXiv:2004.08955*, 2020.
- [14] Hang Zhang, Kristin Dana, Jianping Shi, Zhongyue Zhang, Xiaogang Wang, Amrith Tyagi, and Amit Agrawal. Context encoding for semantic segmentation. In *Proceedings of the IEEE conference on Computer Vision and Pattern Recognition*, pages 7151–7160, 2018.
- [15] Roman Solovyev, Weimin Wang, and Tatiana Gabruseva. Weighted boxes fusion: ensembling boxes for object detection models. *arXiv preprint arXiv:1910.13302*, 2019.
- [16] Less Wright. Ranger-Deep-Learning-Optimizer, 2019.
- [17] Zhi Tian, Chunhua Shen, Hao Chen, and Tong He. Fcos: Fully convolutional one-stage object detection. In *Proceedings of the IEEE/CVF International Conference on Computer Vision*, pages 9627–9636, 2019.
- [18] Kaiming He, Xiangyu Zhang, Shaoqing Ren, and Jian Sun. Deep residual learning for image recognition. In *Proceedings of the IEEE conference on computer vision and pattern recognition*, pages 770–778, 2016.
- [19] Diederik P Kingma and Jimmy Ba. Adam: A method for stochastic optimization. *arXiv preprint arXiv:1412.6980*, 2014.
- [20] Rasmus Rothe, Matthieu Guillaumin, and Luc Van Gool. Non-maximum suppression for object detection by passing messages between windows. In *Asian conference on computer vision*, pages 290–306. Springer, 2014.
- [21] Kai Chen, Jiaqi Wang, Jiangmiao Pang, Yuhang Cao, Yu Xiong, Xiaoxiao Li, Shuyang Sun, Wansen Feng, Ziwei Liu, Jiarui Xu, et al. Mmdetection: Open mmlab detection toolbox and benchmark. *arXiv preprint arXiv:1906.07155*, 2019.

- [22] Liyuan Liu, Haoming Jiang, Pengcheng He, Weizhu Chen, Xiaodong Liu, Jianfeng Gao, and Jiawei Han. On the variance of the adaptive learning rate and beyond. In *Proceedings of the Eighth International Conference on Learning Representations (ICLR 2020)*, April 2020.
- [23] Michael R Zhang, James Lucas, Geoffrey Hinton, and Jimmy Ba. Lookahead optimizer: k steps forward, 1 step back. *arXiv preprint arXiv:1907.08610*, 2019.
- [24] Hongwei Yong, Jianqiang Huang, Xiansheng Hua, and Lei Zhang. Gradient centralization: A new optimization technique for deep neural networks. In *European Conference on Computer Vision*, pages 635–652. Springer, 2020.
- [25] Yelin He, Xianbiao Qi, Jiaquan Ye, Peng Gao, Yihao Chen, Bingcong Li, Xin Tang, and Rong Xiao. Pingan-vcgroup’s solution for icdar 2021 competition on scientific table image recognition to latex. *arXiv*, 2021.
- [26] Jiaquan Ye, Xianbiao Qi, Yelin He, Yihao Chen, Dengyi Gu, Peng Gao, and Rong Xiao. Pingan-vcgroup’s solution for icdar 2021 competition on scientific literature parsing task b: Table recognition to html. *arXiv preprint arXiv:2105.01848*, 2021.